Mutual Coupling Analysis of 6G Ultra-Massive MIMO Channel Measurements and Models

Rui Feng[1,2], Cheng-Xiang Wang[2,1,*], Jie Huang[2,1], Yi Zheng[2,1], Fan Lai[2,1], and Wenqi Zhou[2,1]
[1]Purple Mountain Laboratories, Nanjing, 211111, China.
[2]National Mobile Communications Research Laboratory, School of Information Science and Engineering, Southeast University, Nanjing, 210096, China.
[*]Corresponding Author: Cheng-Xiang Wang
Emails: fengrui@pmlabs.com.cn, {chxwang, j_huang, zheng_yi, lai_fan, wqzhou}@seu.edu.cn

ICC 2022 - IEEE International Conference on Communications | 978-1-5386-8347-7/22/$31.00 ©2022 IEEE | DOI: 10.1109/ICC45855.2022.9839009

***Abstract*—In the sixth generation (6G) wireless communication systems, the employment of ultra-massive multiple-input multiple-output (MIMO) technology can provide significant performance improvement. Meanwhile, it introduces some new channel propagation characteristics. For 6G system design and evaluation, a comprehensive ultra-massive MIMO channel characteristic analysis and an accurate channel modeling methodology are indispensable. In this paper, we emphasize on the joint correlation property analysis between the transmitter (Tx) and receiver (Rx) sides of ultra-massive MIMO channels. Firstly, the Weichselberger model generated based on the mutual coupling matrix of Tx and Rx eigenvectors is introduced and a geometrical based stochastic model (GBSM) is presented. Secondly, an urban ultra-massive MIMO channel measurement campaign at 5.3 GHz is conducted. By splitting the ultra-massive array into several subarrays, the variances of mutual coupling matrices and corresponding power angular spectrums (PASs) along different subarrays are observed. They show great consistency and exhibit evident spatial non-stationarity. Lastly, channel capacities simulated by the Weichselberger model and twin cluster GBSM are compared with that calculated using the sub-channel measurement data. Through the joint optimization of mutual coupling matrix and capacity, GBSM can provide better fitness of real channel measurement data. We also verify that new channel characteristics at Tx/Rx side and between both sides should all be included in future ultra-massive MIMO channel modeling.**

***Index Terms*—Ultra-massive MIMO, channel modeling, spatial non-stationarity, mutual coupling, channel capacity**

I. INTRODUCTION

For the upcoming 6G wireless communications, new technologies should be employed to meet the ever increasing demands of system coverage and capacity [1]–[3]. Ultra-massive MIMO, equipping hundreds to thousands of individual antenna elements at the base station to serve amount of user equipments simultaneously, is envisioned as one of the most promising 6G key technologies. It is able to provide significant improvement of energy efficiency and spectrum efficiency [4], [5]. To benefit the design and evaluation of ultra-massive MIMO systems, accurate channel modeling is of vital importance to provide essential references. It is worth noting that the usage of extra large dimensional antenna array may bring some new channel propagation characteristics. This makes the conventional channel models not suitable any more. Therefore, it is crucial to investigate new ultra-massive MIMO channel characteristics comprehensively and afford reliable instructions for the accurate channel modeling [6], [7].

There are some works focused on the investigation of new (ultra-) massive MIMO channel characteristics. The mostly analyzed channel statistics include the first-order mean and probability density function, as well as the second-order delay/angular spread, auto/cross-correlation function, power spectral density, etc. Based on these channel statistics, spherical wavefront, spatial non-stationarity, and channel hardening are verified from real channel measurement campaigns [8]. It has been shown that signals impinging at the Rx array exhibit spherical wavefront rather than plane wavefront, different antenna elements may see different clusters, and channels among different users tend to show orthogonality. However, the above first- and second-order statistics are only used for channel characterization at either Tx or Rx side, while the joint analysis between Tx and Rx sides are often ignored. As joint Tx and Rx channel characteristics are important for intact system analysis, further investigation of ultra-massive MIMO channel characteristics between Tx and Rx sides is essential.

In existing channel modeling methods, though some of the new channel characteristics have been considered [9]–[11], there is rarely work paying attention to the joint correlation at both sides. In correlation based stochastic models (CBSMs), there are the Kronecker based stochastic model (KBSM) [12], virtual channel representation (VCR) [13], and Weichselberger model [14]. The KBSM assumes Tx independent of Rx, the spatial correlation matrix can be calculated as the kronecker product of one-sided matrices. The VCR transforms the physical domain representation into virtual beam domain and introduces the joint correlation of both sides. To make better sense of mutual coupling matrix, the Weichselberger model replaces the constructed virtual beams of VCR with eigenvectors of one-sided spatial correlation matrices. It has been shown that the involvement of mutual coupling matrices in VCR and Weichselberger model shows significant performance lifting over KBSM, especially in the case of very large array. However, CBSMs can only be used for system-level performance evaluation and the accuracy of CBSMs still need to be improved. For example, the used second-

order spatial correlation matrix may not be enough to describe (ultra-massive) MIMO channels. Though the GBSMs inherent the joint correlation property in the geometry relationships of multipath components (MPCs) with corresponding angle of departure (AoD) and angle of arrival (AoA), the MPCs are randomly paired and not fully specified [15]. That is to say, the mutual coupling constructed by GBSMs should be jointly optimized with the real channel propagation characteristics.

To fill above gaps, we conduct outdoor ultra-massive MIMO channel measurements at 5.3 GHz and focus on the investigation of joint correlation property between Tx and Rx sides. The physical mapping between the coupling matrix and real measurement environment, as well as the variance of mutual coupling along ultra-massive array are analyzed. Performances of several typical channel models in terms of channel capacity are compared and corresponding analyses of mutual coupling based on GBSM are given to show the superiority of existing channel models.

The remainder of this paper is organized as follows. In Section II, the Weichselberger model including the mutual coupling matrix, a twin cluster GBSM, and relevant statistical properties are introduced. In Section III, mutual coupling analysis based on channel measurements and channel models is presented. Finally, conclusions are drawn in Section IV.

II. Wireless Channel Models and Statistical Properties

A. CBSM and Full Correlation Matrix

The fundamental thought behind CBSMs is that the channel coefficients are assumed to be zero-mean complex Gaussian distributed. Therefore, the channel impulse response (CIR) of each CBSM is completely determined by the channel covariance matrix. Assuming a time-invariant MIMO system with M_T and M_R uniform linearly located Tx and Rx antennas. The CIR can be generated as

$$\mathrm{vec}(\mathbf{H})=\mathbf{R}_{\mathrm{MIMO}}^{1/2}\mathrm{vec}(\mathbf{G}) \tag{1}$$

where $\mathrm{vec}(\cdot)$ is the vectorization of matrix. It stacks the columns of $\mathbf{H}$ and turns $\mathbf{H}$ with $M_\mathrm{R} \times M_\mathrm{T}$ dimension into a column vector of size $M_\mathrm{R}M_\mathrm{T} \times 1$. $\mathrm{vec}(\mathbf{G})$ is an i.i.d. zero mean and unit variance vector. It is worth noting that $\mathbf{R}_{\mathrm{MIMO}}$ is the full correlation matrix that describes the inherent spatial structure of MIMO channel. It contains the mutual correlation values among all channel matrix elements,

$$\mathbf{R}_{\mathrm{MIMO}} = \mathbb{E}\left\{\mathrm{vec}(\mathbf{H})\mathrm{vec}^{\mathrm{H}}(\mathbf{H})\right\} \tag{2}$$

where $\mathbb{E}\{\cdot\}$ is the expectation operator and $(\cdot)^{\mathrm{H}}$ is the conjugate transpose.

As $\mathbf{R}_{\mathrm{MIMO}}$ has $M_\mathrm{R}^2M_\mathrm{T}^2$ elements in total, the complexity of using full correlation matrix to get $\mathbf{H}$ is high. In addition, the physical interpretation of $\mathbf{R}_{\mathrm{MIMO}}$ is not certain. Therefore, to give replacements of $\mathbf{R}_{\mathrm{MIMO}}$, KBSM, VCR, and Weichselber model were proposed successively.

B. Weichselberger Model and Mutual Coupling Matrix

Weichselberger model was proposed by W. Weichselberger in 2003 [14]. It inherits the model structure of VCR and considers joint correlation property by using the average coupling between the eigenvectors of Tx and Rx sides. It can be represented as

$$\mathbf{H}_W = \mathbf{U}_\mathrm{R}\left(\tilde{\mathbf{\Omega}} \odot \mathbf{G}\right)\mathbf{U}_\mathrm{T}^{\mathrm{T}} \tag{3}$$

where $(\cdot)^{\mathrm{T}}$ is the transpose operator and $\mathbf{U}_\mathrm{T}$ and $\mathbf{U}_\mathrm{R}$ are eigenbases of one-sided correlation matrices $\mathbf{R}_\mathrm{T}$ and $\mathbf{R}_\mathrm{R}$, respectively. Namely, they can be calculated by the singular value decomposition of $\mathbf{R}_\mathrm{T}$ and $\mathbf{R}_\mathrm{R}$,

$$\mathbf{R}_\mathrm{T} = \mathbb{E}\left\{\mathbf{H}^{\mathrm{T}}\mathbf{H}^{*}\right\} = \mathbf{U}_\mathrm{T}\mathbf{\Lambda}_\mathrm{T}\mathbf{U}_\mathrm{T}^{\mathrm{H}} \tag{4}$$

and

$$\mathbf{R}_\mathrm{R} = \mathbb{E}\left\{\mathbf{H}\mathbf{H}^{\mathrm{H}}\right\} = \mathbf{U}_\mathrm{R}\mathbf{\Lambda}_\mathrm{R}\mathbf{U}_\mathrm{R}^{\mathrm{H}}. \tag{5}$$

In (3), $\tilde{\mathbf{\Omega}}$ is the coupling matrix of Tx and Rx eigenvectors. The coefficients of $\tilde{\mathbf{\Omega}}$ can be obtained through square root extraction of $\mathbf{\Omega}$,

$$\mathbf{\Omega} = \mathbb{E}\left\{\left(\mathbf{u}_\mathrm{R}^{\mathrm{H}}\mathbf{H}\mathbf{u}_\mathrm{T}^{*}\right) \odot \left(\mathbf{u}_\mathrm{R}^{\mathrm{T}}\mathbf{H}^{*}\mathbf{u}_\mathrm{T}\right)\right\} \tag{6}$$

where $(\cdot)^{*}$ is the conjugate operator and $\mathbf{u}_\mathrm{T}$ and $\mathbf{u}_\mathrm{R}$ are eigenvectors consisted in $\mathbf{U}_\mathrm{T}$ and $\mathbf{U}_\mathrm{R}$, respectively. The $\tilde{\mathbf{\Omega}}$ specifies the mean amount of energy that is coupled from the eigenvector of Tx side to the eigenvector of Rx side. In [14], it was also verified that $\tilde{\mathbf{\Omega}}$ can reflect the spatial arrangement of scattering objects.

C. Twin Cluster GBSM

In this paper, we take a newly proposed general twin cluster GBSM as an example [10]. It considers space-time-frequency non-stationarity, spherical wavefront, and time variant motion of the Tx, Rx, and scatterers. It is able to be used to multiple scenarios and multiple frequency bands. By setting appropriate model parameters, this model can be applied to massive MIMO channels.

Considering both line-of-sight (LoS) and non-LoS (NLoS) components, the CIR of the q-th receive antenna and p-th transmit antenna at time t can be written as

$$h_{qp}(t) = \sqrt{\frac{K}{K+1}}h_{qp}^{\mathrm{LoS}}(t) + \sqrt{\frac{1}{K+1}}h_{qp}^{\mathrm{NLoS}}(t) \tag{7}$$

where K is the Ricean factor denoting the ratio between the LoS and NLoS powers.

The LoS and NLoS components h_{qp}^{LoS} and h_{qp}^{NLoS} can be expressed according to geometrical relationships and random distributions. Specially, the NLoS components are represented by one-to-one pair clusters and the propagation between paired cluster is abstracted by virtual link. Only when the delay of virtual link is zero, the single-bounce rays can be degenerated from multi-bounce rays. This model can be used to link-level analysis. More details can be found in [10].

D. Statistical Properties

In order to analyze the joint correlation characteristics between Tx and Rx, we consider statistical properties that link and include both ends. Such as PAS, coupling matrix distance (CMD), and channel capacity.

1) PAS: PAS can be used to link Tx and Rx sides together and to observe the joint power distribution over AoAs and AoDs. An efficient way to get PAS is to use the Capon's beamformer [16]. It can not only maximize the beam over desired directions, but also able to minimize the beam over undesired directions. Consider azimuth AoA ϕ_{T} and AoD ϕ_{R} only, the constructed so-called "power spectrum" can be expressed as

$$\mathbf{P}(\phi_{\mathrm{T}},\phi_{\mathrm{R}}) = \frac{1}{\mathbf{a}^{\mathrm{H}}(\phi_{\mathrm{T}},\phi_{\mathrm{R}})\mathbf{R}^{-1}_{\mathrm{MIMO}}\mathbf{a}(\phi_{\mathrm{T}},\phi_{\mathrm{R}})} \tag{8}$$

with $\mathbf{a}(\phi_{\mathrm{T}},\phi_{\mathrm{R}})$ is the vectorization of steering vectors in direction ϕ_{R} and ϕ_{T}. PAS can also be calculated by using the high resolution space alternating generalized maximization-expectation algorithm (SAGE). However, SAGE algorithm has higher computational complexity.

2) CMD: In [17], other metrics including channel capacity, diversity measure, and CMD were proposed to compare KB-SM, Weichselberger model, and VCR with two independent measurement campaigns at 2 and 5 GHz. Among them, the CMD measures the similarity between different correlation matrices at different time instants. In this paper, we calculate the CMD between the i-th and j-th subarray coupling matrices,

$$D_{i,j} = 1 - \frac{\mathrm{vec}^{\mathrm{H}}(\mathbf{\Omega}_i)\mathrm{vec}(\mathbf{\Omega}_j)}{\|\mathrm{vec}(\mathbf{\Omega}_i)\|_2 \|\mathrm{vec}(\mathbf{\Omega}_j)\|_2} \tag{9}$$

with $\|\cdot\|_2$ denotes the norm. If $D_{i,j} = 0$, the coupling matrices are equal; if $D_{i,j} = 1$, they differ to a maximum amount. In this paper, i is set to 1. That means, Ω_1 is set as a basis, all coupling matrices will be compared with the first subarray to observe the variances along ultra-massive array.

3) Channel Capacity: Systematic performance can be measured by channel capacity, bit error rate, etc. Considering the single-user case, without channel knowledge at Tx side, the channel capacity with equal power allocation scheme can be calculated as

$$C = \mathbb{E}\left\{\log_2\left[\det\left(\mathbf{I} + \frac{\rho}{M_{\mathrm{T}}}\bar{\mathbf{H}}\bar{\mathbf{H}}^{\mathrm{H}}\right)\right]\right\} \quad (\mathrm{bps/Hz}) \tag{10}$$

where det $(\cdot)$ denotes the determinant operation, $\mathbf{I}$ is the unit matrix, ρ is the signal-to-noise ratio (SNR), and $\bar{\mathbf{H}}$ is the normalized channel matrix,

$$\bar{\mathbf{H}} = \mathbf{H}_W\left\{\frac{1}{M_{\mathrm{T}}M_{\mathrm{R}}}\sum_{qp}|h_{qp}|^2\right\}^{-\frac{1}{2}} \tag{11}$$

where h_{qp} denotes the CIR of the q-th receive antenna and p-th transmit antenna.

(a) Real channel measurement environment

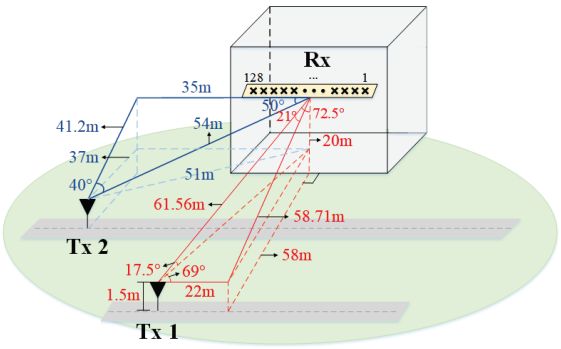

(b) Abstracted channel measurement setups

Fig. 1. Channel measurements in an urban environment at 5.3 GHz.

III. Measurement and Simulation Analysis

A. Ultra-massive MIMO Channel Measurement Campaigns

The ultra-massive MIMO channel measurement campaigns are conducted in an urban environment at China Network Valley, Jiangsu Province. The carrier frequency is 5.3 GHz and the bandwidth is 160 MHz. The real measurement environment and the simplified geometrical relationship between Tx and Rx are illustrated in Fig. 1. During channel measurements, the channel is seemed as static.

At the Rx side, an ultra-massive array with 128 elements is constructed. It stretches out up to 4.3 m with adjacent antenna elements spacing 0.6 wavelength. It is elevated to the outside wall of the building with 20 meters high. At the Tx side, 8 omnidirectional antennas are positioned on the truck with the height about 1.5 m. Two locations of Tx, i.e., Tx 1 and Tx 2, are selected to stand for LoS and NLoS cases. The surroundings at Tx 1 and Tx 2 are depicted in Fig. 1(a). It can be seen that Tx 1 is concealed by many trees, the direct path between Tx 1 and Rx is blocked by leaves. Tx 2 is placed at an open area of the parking lot. Though Tx 2 can be directly seen by the Rx array, there are cars and bus nearby, as well as trees in between. According to the coordinates of Tx and Rx, relative distances and angles are indicated in Fig. 1(b).

B. PAS Variances and Spatial Non-stationarity

As the Rx array aperture L is 4.3243 m and the wavelength λ is 0.0566 m, the corresponding Rayleigh distance is calculated as $2L^2/\lambda = 660.7622$ m. Therefore, Tx 1 and Tx 2 are both within the Rayleigh distance. For the convenience

of following analysis, we divide the whole array into several subarrays, each subarray contains 10 antenna elements. Then, far-field wavefront condition can be satisfied.

The variances of PAS over ultra-massive linear array at Tx 1 and Tx 2 are shown in Fig. 2. Here, we select three subarrays with antenna indices 21–30, 61–70, and 101–110 to get PASs. They are representative for the statistical properties at two ends and middle of the ultra-massive array. For fair comparison, we set the upper bound of z-axis as 1.3×10^{-5}.

It can be seen in Figs. 2(a)–2(c) that PASs show obvious variances, i.e., from two distinct peaks to several peaks and then to four peaks. In addition, the MPCs spread in AoA domain, while center at AoD domain arround $69°$. Affected by leaves, signals transmitted from Tx 1 impinge at Rx with wide angular range. This angle floats at different subarrays. In Figs. 2(d)–2(f), it can be seen that MPCs center at AoD domain with $49°$ roughly. Obvious variances can be observed at different subarrays. Besides the LoS path, the wide spread angles are also caused by surrounding trees and buildings. It can be concluded that in both cases, distinct spatial non-stationarity can be found in ultra-massive MIMO channels. The shift of LoS angle also shows spherical wavefront property.

C. Mutual Coupling Variances and Spatial Non-stationarity

In Fig. 3, the mutual coupling matrices for three subarrays of Tx 1 and Tx 2 are shown. For comparison convenience, we fix the upper bounds of z-axis for Tx 1 and Tx 2 as 2×10^{-3} and 1.6×10^{-2}, respectively. From Fig. 3(a), it can be seen that there are two strong eigenvectors at the Tx side coupled into only one Rx eigenvectors. The peak number is coincide with that in Fig. 2(a). This also represents that main scatterers are distributed at the Tx side. In Figs. 3(b) and 3(c), the histograms are transitioned to several peaks and several transmit eigenvectors coupled to several receive eigenvectors. The coupling energies become weaker than that in Fig. 3(a). It can be deduced that there are rich MPCs and scatterers are distributed around Tx rather than Rx. Compared with the corresponding PASs, the number of peaks shows consistence. Refer to the measurement environment, this scatterer should be constructed by surrounded plants. In Figs. 3(d)–3(f), a clear dominant transmit eigenvector is coupled to a receive eigenvector. The coupling energy is much larger than that in the NLoS case. Actually there are also weaker transmit eigenvectors coupled to the receive eigenvector. This specifies an obvious LoS case and means scatterers are located at the Tx side. In addition, there are differences among three subarrays.

To have an in-depth observation of the mutual coupling variances along ultra-massive array, we employ a sliding window with size 10 to constructed 119 subarrays. In Fig. 4, the CMDs are calculated between coupling matrices of the first subarray and all 119 subarrays for Tx 1 and Tx 2 cases. It is evident to seen that the LoS scenario shows lower and smoother variances than that of the NLoS scenario. For the NLoS case, there are several peaks, they may caused by non-uniform distributed scatterers at Tx side. They show evident change of channel condition. In general, both scenarios show slight increases with the distance expansion of subarrays.

We conclude that the mutual coupling matrices show alignment with the PASs. Though the peaks of mutual coupling are not actually corresponding to signal directions, the numbers of peaks are basically the same with that in the PASs. Therefore, mutual coupling matrices can also be used to show the spatial

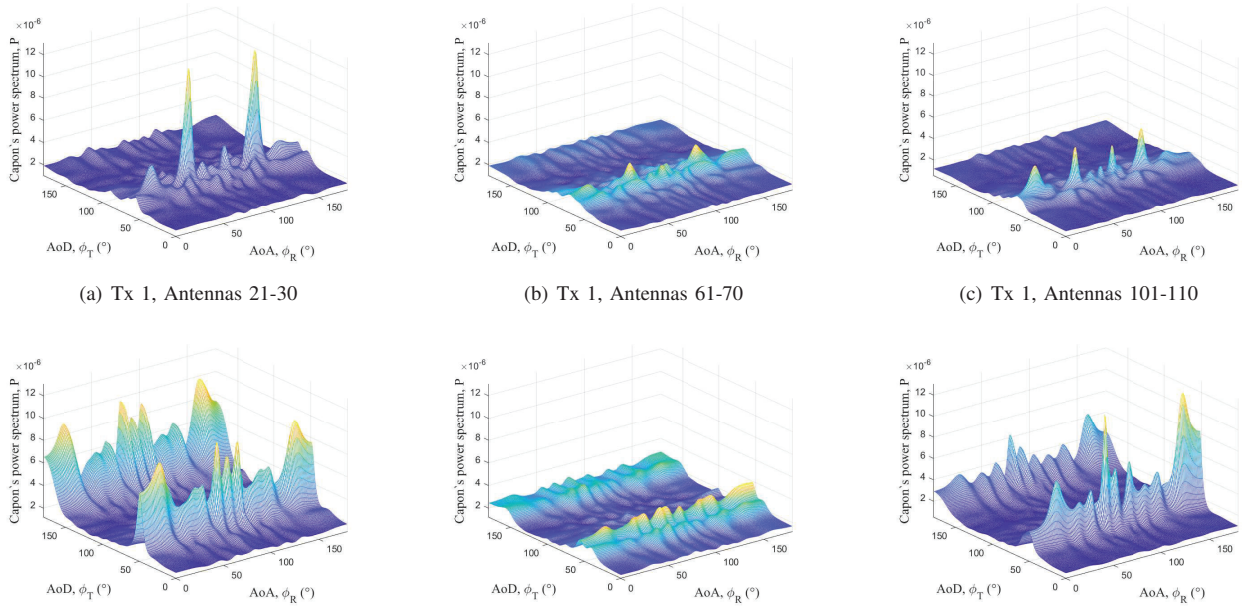

(a) Tx 1, Antennas 21-30 (b) Tx 1, Antennas 61-70 (c) Tx 1, Antennas 101-110

(d) Tx 2, Antennas 21-30 (e) Tx 2, Antennas 61-70 (f) Tx 2, Antennas 101-110

Fig. 2. Variances of PAS over ultra-massive array at Tx 1 and Tx 2.

non-stationarity property. In addition, the rough scatterers distribution can be inferred accordingly.

D. Simulation Analysis of Channel Models

In Fig. 5, we select measurement data of any subarray, e.g. with antennas 101–110 at Tx 1, to calculate channel capacity. In order to show the superiority of the inclusion of mutual coupling, channel capacities calculated based on KBSM and Weichselberger model are generated, as well as that of using the full correlation matrix. The simulated channel capacity of GBSM is given by optimizing parameters to fit with measurement result. The model parameters are set as $M_R = 128$, $M_T = 8$, $f_c = 5.3$ GHz, $D = 60$ m, $\sigma_{AoA} = 10$, $\sigma_{AoD} = 4$.

It can be seen that KBSM underestimates the calculated measurement channel capacities with significant error, this is because it ignores the joint correlation at Tx and Rx sides. The performance of Weichselberger model is perfectly matched with that of using full correlation matrix. It shows good matching of mutual coupling measure with full correlation matrix and shows privilege of Weichselberger model over KBSM. However, it fails to provide accurate channel capacity approximation. This reminds us that the usage of second order statistics may not enough to characterize wireless channels.

Through parameter optimization, it is shown that channel capacity simulated using the twin cluster GBSM can well approximate that calculated using the real channel measurement data. The coupling energy between Tx and Rx eigenvectors is jointly optimized. The result is shown in Fig. 6. It can be seen that the corresponding mutual coupling distribution is reasonable and well matched with that of Figs. 3(d). Only one Tx eigenvector is strongly coupled with one Rx eigenvector. Therefore, we can see that parameter optimization of GBSM can also include the impact of mutual coupling into consideration.

IV. Conclusions

In this paper, mutual coupling analysis of channel measurements and models has been presented. Based on urban ultra-massive MIMO channel measurements, the spatial non-stationarity has been verified with both PAS and mutual coupling matrix by separating the whole array into subarrays. It has shown that the mutual energy coupling between Tx and Rx sides is related to PAS and can be used to ascertain the distribution of dominant scatterers. In addition, the LoS scenario has lower CMD variance than the NLoS scenario. Through channel capacity simulation from the KBSM, Weichselberger model, full correlation matrix, and GBSM with that calculated from the measurement data, it has shown that the twin cluster GBSM can provide the overall best fitted results. The analysis of mutual coupling matrix for the twin cluster GBSM has further revealed the superiority of joint correlation description. We have drawn conclusions that the mutual coupling between Tx and Rx sides should be taken into account when optimizing model parameters to characterize real wireless channels and be considered in future wireless channel modeling.

Acknowledgement

This work was supported by the National Key Research and Development Program of China under Grant 2018YFB1801101, the National Natural Science Foundation of China (NSFC) under Grant 61960206006 and Grant 61901109; the

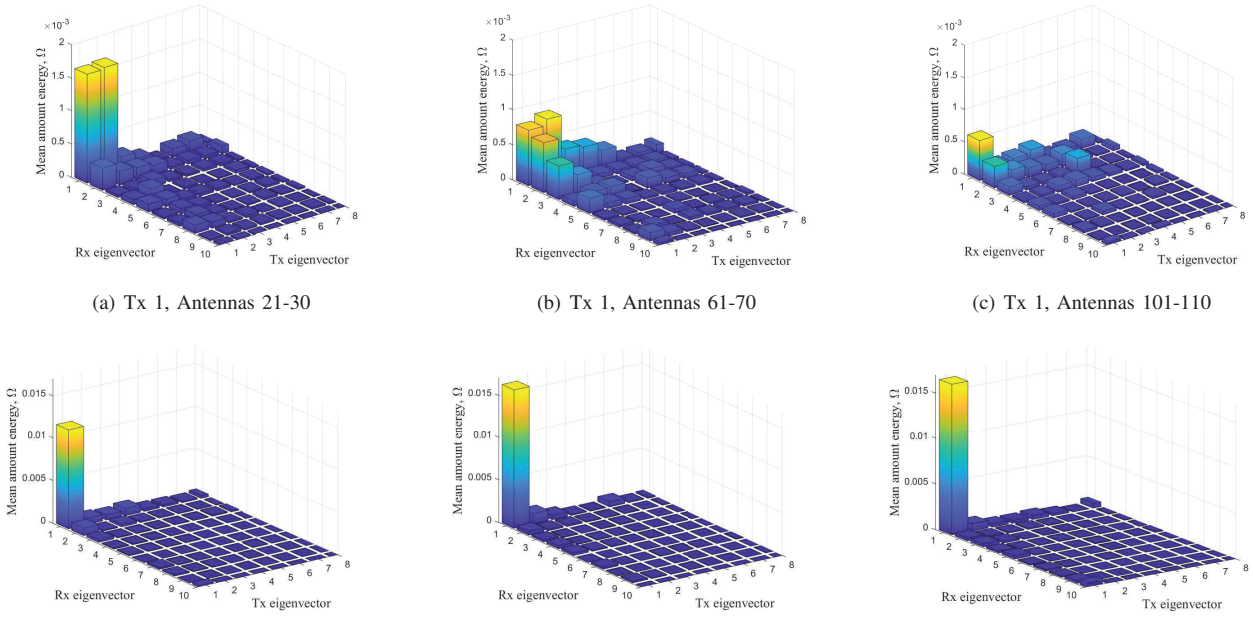

(a) Tx 1, Antennas 21-30 (b) Tx 1, Antennas 61-70 (c) Tx 1, Antennas 101-110

(d) Tx 2, Antennas 21-30 (e) Tx 2, Antennas 61-70 (f) Tx 2, Antennas 101-110

Fig. 3. Variances of coupling matrix over ultra-massive array.

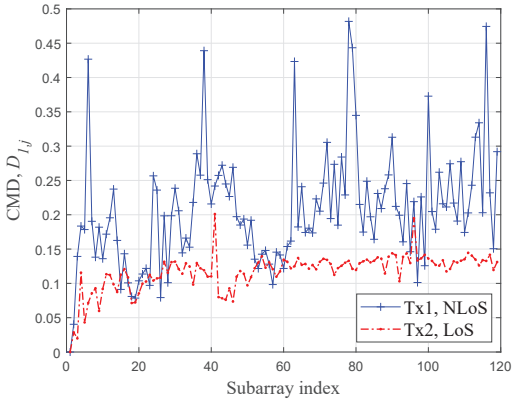

Fig. 4. CMDs of the LoS and NLoS scenarios.

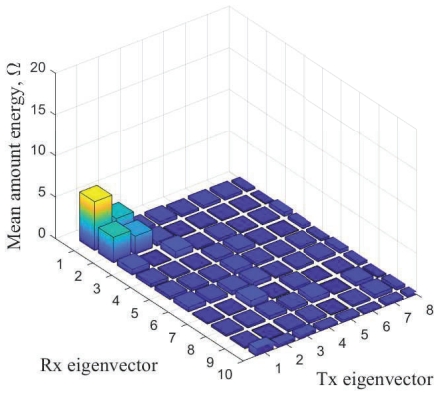

Fig. 6. Mutual coupling of the twin cluster GBSM.

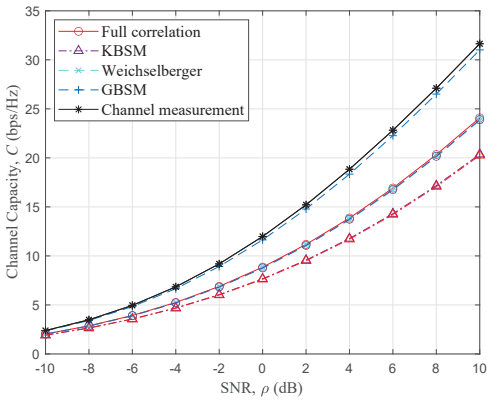

Fig. 5. Channel capacities calculated using different channel models.

Frontiers Science Center for Mobile Information Communication and Security; the High Level Innovation and Entrepreneurial Research Team Program in Jiangsu; the High Level Innovation and Entrepreneurial Talent Introduction Program in Jiangsu; the Research Fund of National Mobile Communications Research Laboratory, Southeast University, under Grant 2021B02; the EU H2020 RISE TESTBED2 Project under Grant 872172; the Fellowship of China Postdoctoral Science Foundation under Grant 2021M690628; and the Natural Science Foundation of Shandong Province under Grant ZR2019PF010.

REFERENCES

[1] X.-H. You, C.-X. Wang, J. Huang, et al., "Towards 6G wireless communication networks: Vision, enabling technologies, and new paradigm shifts," *Sci. China Inf. Sci.*, vol. 64, no. 1, Jan. 2021, doi: 10.1007/s11432-020-2955-6.

[2] E. D. Carvalho, A. Ali, A. Amiri, M. Angjelichinoski, and R. W. Heath, "Non-stationarities in extra-large-scale massive MIMO," *IEEE Wireless Commun.*, vol. 27, no. 4, pp. 74–80, Aug. 2020.

[3] Á. O. Martínez, E. De Carvalho, and J. ∅. Nielsen, "Towards very large aperture massive MIMO: A measurement based study," in *Proc. IEEE GlobeCom Wkshps' 14*, Austin, USA, Dec. 2014, pp. 281–286.

[4] E. Björnson, L. Sanguinetti, H. Wymeersch, J. Hoydis, and T. L. Marzetta, "Massive MIMO is a reality—What is next? Five promising research directions for antenna arrays," June 2019. [Online]. Available: https://arxiv.org/abs/1902.07678

[5] F. Rusek, D. Persson, B. K. Lau, E. G. Larsson, T. L. Marzetta, O. Edfors, and F. Tufvesson, "Scaling up MIMO: Opportunities and challenges with very large arrays," *IEEE Signal Process. Mag.*, vol. 30, no. 1, pp. 40–60, Jan. 2013.

[6] C.-X. Wang, J. Huang, H. M. Wang, X. Q. Gao, X. H. You, and Y. Hao, "6G wireless channel measurements and models: Trends and challenges," *IEEE Veh. Techn. Mag.*, vol. 15, no. 4, pp. 22–32, Dec. 2020.

[7] X. Gao, O. Edfors, F. Rusek, and F. Tufvesson, "Massive MIMO performance evaluation based on measured propagation data," *IEEE Trans. Wireless Commun.*, vol. 14, no. 7, pp. 3899–3911, July 2015.

[8] P. Zhang, J. Q. Chen, X. L. Yang, N. Ma, and Z. Zhang, "Recent research on massive MIMO propagation channels: A survey," *IEEE Commun. Mag.*, vol. 56, no. 12, pp. 22–29, Dec. 2018.

[9] C.-X. Wang, J. Bian, J. Sun, W. Zhang, and M. Zhang, "A survey of 5G channel measurements and models," *IEEE Commun. Surveys Tuts.*, vol. 20, no. 4, pp. 3142–3168, 4th Quart., 2018.

[10] J. Bian, C.-X. Wang, X. Q. Gao, X. H. You, and M. G. Zhang, "A general 3D non-stationary wireless channel model for 5G and beyond," *IEEE Trans. Wireless Commun.*, vol. 39, no. 4, pp. 3211–3224, May 2021.

[11] S. B. Wu, C.-X. Wang, H. Aggoune, M. M. Alwakeel, and X. You, "A general 3D non-stationary 5G wireless channel model," *IEEE Trans. Commun.*, vol. 66, no. 7, pp. 3065–3078, July 2018.

[12] C. N. Chuah, J. M. Kahn, and D. Tse, "Capacity of multi-antenna array systems in indoor wireless environment," in *Proc. IEEE GLOBECOM' 98*, Sydney, Australia, Nov. 1998, pp. 1894–1899.

[13] A. M. Sayeed, "Deconstructing multiantenna fading channels," *IEEE Trans. Signal Process.*, vol. 50, no. 10, pp. 2563–2579, Oct. 2002.

[14] W. Weichselberger, M. Herdin, H. Özcelik, and E. Bonek, "A stochastic MIMO channel model with joint correlation at both link ends," *IEEE Trans. Wireless Commun.*, vol. 5, no. 1, pp. 90–100, Jan. 2006.

[15] Y. Zheng, L. Yu, R. Yang, and C.-X. Wang, "A general massive MIMO GBSM for 6G communication systems," in *Proc. IEEE WCNC'21*, Nanjing, China, Apr. 2021.

[16] H. Krim and M. Viberg, "Two decades of array signal processing research: The parametric approach," *IEEE Signal Proc. Mag.*, vol. 13, no. 4, 1996, pp. 67–94.

[17] E. Bonek, "Experimental validation of analytical MIMO channel models," *Electrical Engineering Inform. Technol.*, vol. 122, no. 6, pp. 196–205, June 2005.